EXPERIMENTAL AND NUMERICAL STUDY OF SHORT HOT JET DIFFUSERS

M.Amielh*, M. Cantillon**, M.P. Chauve*
* CNRS Research Officers
Institut de Mécanique Statistique de la Turbulence
12 avenue du Général Leclerc, 13003 Marseille, FRANCE
** Engineer
EUROCOPTER FRANCE, département Aéromécanique
13725 Marignane Cedex, FRANCE

ABSTRACT

Comparisons between experimental and numerical results are obtained in the study of short hot jet diffusers developed for gas mixing at engine exhausts. The experimental investigations of three diffusers of more and more complex geometry are used to calibrate two codes both characterized by a k-ε model for the turbulence closure. The first is a two-dimensional code based on finite volume discretization, while the second is a three-dimensional code using the finite element method. The velocity, temperature and pressure fields are measured with various complementary technics such as hot-wire, LDA or clinometric pressure probes. Comparisons of calculated and experimental results show that the three-dimensional code is more suitable for describing the complex flow behavior inside the diffuser, especially when mean pressure variation is concerned.

Introduction

Dilution of hot jets is of great interest in many industrial applications, in particular for the engine exhausts where the main objective is often to increase gas mixing at the outlet. These improvements are obtained by adding a diffuser at the nozzle outlet and by diluting the hot jet with external fresh air. Thus, a compromise between the increased thermal exchanges and the flow "quality", linked for example to the pressure performance, had to be taken into account in most of the proposed diffuser geometries, themselves depending on the factors of weight and overall dimensions, especially when helicopters are considered. Therefore modeling is very useful in order to check the optimal configuration, because the several experimental models time and money. However, since the problems related to industrial application are quite far removed from normal basic experiments performed on variable mass jets or diffusers, the results found in the literature on these topics do not allow us to predict the precise behavior of the heated flow in a short diffuser. Suitable experiments were used for this study. These experiments should provide a detailed data base for validation of these codes and enable us to analyze the complex behavior of the internal flow within diffusers. Therefore three diffusers were selected to gradually introduce the geometrical complexities that are reflected in the behavioral patterns of internal flow, which are more and more difficult to reproduce numerically. The aim of this paper is to present these three jet diffuser experiments used for the validation of two codes intended, among other things, for optimal streamlining of industrial diffusers.

The flows studied are turbulent, subsonic and sometimes at very high temperatures. Therefore these conditions required suitable measurement technics, which are described firstly. The specific features of the two numerical codes are then explained. The performance data of the two codes are compared with the experimental results to verify their validation.

Experimental set-up

Experimental facilities

The double flux mixing experiments described herein are performed in a horizontal wind tunnel(1) on a 6 x 3 m^2 surface, 2.5 m high (fig. 1).

The primary flow that simulates the outlet nozzle flow is supplied by a centrifugal blast V_1. The arrangement is conceived so that an axisymmetric or plane primary nozzle can be used. Moreover, the primary flow can be heated up to 673K by a 45kW controlled heating box. The nominal conditions that are maintained for the whole presented experiment square with a Mach number equal to 0.15 on the axis of the primary nozzle outlet. The primary flux is adjusted by an electronic speed variator installed on the V_1 blast motor. According to the considered cases, the Reynolds

number based on the axial velocity at the primary nozzle outlet varies in the range 60000-160000.

The secondary flow used in mixing is entrained by the primary jet and by a downstream blower, located behind the outlet box that simulates the infinite outlet conditions. The choice of the secondary flux is determined, firstly, by the secondary/primary cross-section ratio S_2/S_1 and secondly, by the variable speed belt drive set up on the V_2 blast motor. Other control facilities are also obtained by putting filters on the secondary flow intake or by opening shutters on the upstream face of the outlet box in order to adjust the internal depression using these different devices. Thus the secondary/primary volume flux ratio may be varied continuously in the range 0-2. In general, both flows are mixed beyond the primary nozzle outlet in a model called the "diffuser". Although the presented geometries are very different, some joint characteristics are observed. Indeed, it can be noted that all the described diffusers are made with a first constant cross-section pipe followed by a divergent pipe where a longitudinal pressure gradient is induced. The specificity of these diffusers is also related to their short length ($L/D_2<5$) compared to the usual basic experiments or calculations[2,3,4] ($L/D_2\approx100$). Therefore, in the present experiments, mixing is not totally effective before the diffuser outlet and it shows eccentric and complex behavior, such as reversal flow near the diffuser wall.

Models

Axisymmetric diffuser (AX) The axisymmetric diffuser model is the most simple studied geometric configuration[1] (fig. 2). The primary jet is ejected from an axisymmetric nozzle with a D_1=50mm diameter. The diffuser's intake diameter is D_2=100mm so that the secondary intake cross-section verifies S_2/S_1=3. The cross-section of the diffuser is circular and constant throughout a length of 110mm. The second part of the diffuser is divergent with an outlet diameter D=140mm for a 7.9° total aperture angle. Therefore the outlet/intake cross-section ratio of the diffuser is 1.96 and its total length is L=400mm. The nozzle and the diffuser are constructed in stainless steel in order to bear a 673K temperature.

Two-dimensional plane diffuser (2D) In this case, the cross-section of the primary nozzle and of the diffuser are rectangular[5] (fig. 3). The aspect ratio of the primary jet defined by a (a=height D_1 /width l) is 5 (D_1=20mm, l=100mm). In this configuration, the secondary flow is divided into an upper and a lower flux on both sides of the primary jet. As the height of the diffuser's intake is D_2=80mm with a l=100mm width; the secondary cross-section is such that S_2/S_1=3 too. The diffuser's cross-section is constant in its upstream part throughout a length of 200mm. The second part of the diffuser is a 90° bent pipe. Its divergent section with an internal deflector strip drives the mixed flow to the horizontal outlet section.

The outlet/intake cross-section ratio of the diffuser is 1.5. Its total length is L=388mm. As in the previous model, the two-dimensional plane diffuser is in stainless steel.

Three-dimensional diffuser (3D) This model is a 1/4 scale industrial diffuser[6] (fig. 4). The primary jet is ejected from a nozzle. The nozzle's outlet cross-section has a "daisy" shape composed of 12 radial "petals" arranged around a central circle of 66 mm diameter within an external diameter of D_2=100mm. Due to the necessity to match the industrial conditions, a central core is placed inside the "daisy" in order to simulate the turbine axis. This internal core, which forces the air supply inside the petals, has a 35mm diameter in the outlet section of the primary nozzle. The diffuser has a circular cross-section with a 100mm constant diameter, and is 58mm long. The downstream part is a 83° bent pipe with a divergent section characterized by a 2.5 outlet/intake cross-section ratio. The total length of the diffuser is 363mm. The "daisy" nozzle is in aluminium. The central core is in wood. The 3D diffuser is machined by a computer-controlled tool in a Plexiglas block.

Probes and procedures

Due to the complexity of the studied flows, various complementary experimental technics are used [1,5]. Indeed, for each geometric configuration, the object is to get the complete mean field of velocity, pressure and temperature (heating case) and also the turbulent intensity profiles of velocity and temperature, for two purpose, (i) to deduce the mixing characteristics; (2) to provide data base for the different code validation. For each probe, a fitted traversing system (accurate to within 1/100 mm in the transverse direction and 1/10 mm in the longitudinal direction) is used. They are connected to a device including a step-by-step motor and an optical encoder with digital readout of distances. Note that the main encountered difficulties were related to the measurement region 's accessibility, due to the

diffuser geometry and to the experimental conditions which required probes and supports bearing high velocities and temperature respectively about 50 m/s and 673K.

The complete measurements are stored in a microcomputer with a well-suited acquisition card.

Pressure measurements In the case where the streamlines are practically not deviated from the diffuser axis direction, the mean pressures are measured with usual total head and static pressure tubes connected to Furness digital micro-manometers working in the scale ±20 or ±200 mm water column. In particular, these probes were used in order to determine the velocity field in the axisymmetric diffuser.

On the other hand, when some flow regions present strong streamline deviation with regard to the diffuser axis direction, a five hole clinometric probe(7) connected to the same micro-manometers is used. After a preliminary calibration for the angle and velocity probe response, the direction and the modulus of the mean velocity vector are obtained using this special probe, especially in the 2D and 3D diffusers. This probe is built so that its pliable support can always be adapted to the wall shape in each investigated section.

Hot wire anemometry Some velocity turbulent intensity measurements are made with hot wires in order, more particularly, to give some indications for the turbulent kinetic energy k initialization in codes. X-crossed hot wires (90°), with a 1.25 mm length and a 5 μm diameter, are used in the 2D diffuser with an overheating aw=0.6. Thus the U and V components of the velocity vector are obtained.

A double probe with a straight wire (diameter 5 μm, length 1.4 mm, aw =0.8) and an upstream cold wire (diameter 1.2 μm, length 0.6 mm, constant current 0.9 mA, gap 0.3 mm) is used to detect reverse flows which occur near the wall diffuser in the separating zone of the flow. So some conditional velocities are deduced from a statistic treatment of the cold wire's intermittent temperature signal when this wire is in the thermal wake of the hot wire due to the flow reversals. Some results obtained with this procedure are presented for the flow in the axisymmetric diffuser.

Laser Doppler anemometry This technic is used only for the velocity measurements inside the 3D diffuser(8). They are performed with a Spectra Physics laser source (15 W continuous, 5 W used), adjusted to the wavelength, λ (=514.5 nm). It is mounted with a monodimensional optical head working in back scatter detection with a 40 MHz Bragg cell. The light is transmitted from the source to the emission-reception head by 20m long optical fibers. The Doppler bursts are processed by a Burst Spectrum Analyzer (Dantec). The primary stream is seeded by a ricin oil aerosol laterally injected in the primary flow in a section located at $10D_2$ upstream from the diffuser intake section. The optical head is mounted on a traversing mechanism with several degrees of freedom (3 translations, 3 rotations) used to simultaneously optimize the adjustments of the laser beams and the probe volume displacement. Some lateral plane glass windows were set up on the 3D diffuser walls to allow proper transmission and reception of the light signal.

With this whole device, one velocity component located in the beam plane and parallel to the diffuser wall is obtained in each investigated section. With a $\pi/2$ rotation of this plane, a second velocity component is measured at the same point. Note that the statistic process is made with 7000 bursts.

Mean temperature measurements They are performed using a type K thermocouple whose sensor probe is 0.8 mm in diameter. The cold reference source is the melting ice.

Numerical approach

Governing equation

The studied flows are mixtures of two coaxial jets of high Reynolds number and low Mach number and possibly in the presence of major heat transfers.

The equations for modeling such flows are therefore Navier-Stokes equations, associated with a turbulence model and possibly an energy equation(9). Considering the assumptions of low Mach number and low pressure variations in relation to the static pressure observed in these flows, we consider that the variations in density only depend on temperature. In addition, because of the industrial nature of the study, the two equations model (k,ε) was chosen for the turbulence model.

Therefore the general system to be resolved is as follows:

Navier-Stokes equations (1)

$$\begin{cases} \left\{ \dfrac{\partial \rho \underline{v}}{\partial t} + (\underline{v}.\underline{\mathrm{grad}})\rho \underline{v} \right\} = -\underline{\mathrm{grad}}\, p + \mathrm{div}\left[\mu \underline{\mathrm{grad}}\, \underline{v}\right] \\ \mathrm{div}\rho \underline{v} = 0 \end{cases}$$

Enthalpy equation (2)

$$\left\{ \frac{\partial \rho T}{\partial t} + (\underline{v}.\underline{\mathrm{grad}})\rho T \right\} = \mathrm{div}\left[\left(\frac{\mu}{Pr} + \frac{\mu_t}{Pr_t} \right) \underline{\mathrm{grad}}\, T \right]$$

k-ε Model (3)

$$\left\{\frac{\partial \rho k}{\partial t}+(\underline{v}.\underline{\mathrm{grad}})\rho k\right\}=\mathrm{div}\left[\left(\mu+\frac{\mu_t}{\sigma_t}\right)\underline{\mathrm{grad}}\,k\right]+P-\rho\varepsilon$$

$$\left\{\frac{\partial \rho \varepsilon}{\partial t}+(\underline{v}.\underline{\mathrm{grad}})\rho\varepsilon\right\}=\mathrm{div}\left[\left(\mu+\frac{\mu_t}{\sigma_\varepsilon}\right)\underline{\mathrm{grad}}\,\varepsilon\right]+C_{\varepsilon 1}\frac{\varepsilon}{k}P-\rho C_{\varepsilon 2}\frac{\varepsilon^2}{k}$$

$P=2\mu_t\,\mathrm{tr}(\underline{\underline{dd}})$ with $\mu_t=\rho C_\mu\frac{k^2}{\varepsilon}$

$Pr_t=0.7$ and $C_{\varepsilon 1}, C_{\varepsilon 2}, C_\mu$ usual constants

$\underline{\underline{d}}$ strain rate tensor

Two numerical codes were used for studying these flows; they are presented below.

PATC code

The PATC code was developed by Eurocopter France[9,10], on the basis of the work of Jones and Launder. It is a finite volume code, used to resolve the above equations for stationary two-dimensional flows (axisymmetric or plane). We use a curvilinear orthogonal mesh in which are defined grids that are shifted in velocity and pressure. A hybrid scheme is used for the diffusion-convection terms, and the velocity-pressure combination is handled by the SIMPLE algorithm. The iterative resolution of the system is performed with the aid of a tridiagonal algorithm.

N3S code

N3S, developed by the Research and Design Department of Electricité de France (France's national electricity supply agency) and the Simulog company, is a flow mechanics code based on the finite element method which is used to handle axisymmetric, planar 2D or 3D geometries[6,11].

The 2.1 (or 3.0) version used here solves the non-stationary Navier-Stokes equations, also coupled to the above described turbulence model. The software package has additional possibilities such as a thermal equation for a passive contaminant and a convective diffusion type equation with source terms and general boundary conditions for additional passive contaminants.

The time scheme uses a separation method, accurate in the first or second order, with a convection equation treatment using a characteristic method which induces a natural eccentricity. A resolution based on finite elements is used for the diffusion and propagation terms. The generalized Stokes problem is solved by a preconditioned Uzawa algorithm[9].

The linear system is determined by conjugate gradient technics which reduce the calculation time and the occupied memory.

Considered geometries and grids

The intake section of the calculation domain is the section where the primary and the secondary flow meet in each studied diffuser. The outlet section of this domain is the real outlet section of the diffuser except for the plane 2D diffuser for which the calculation limits are extended in relation to the experimental domain. This precaution is necessary to take into account the fact that the flows separated by the deflector strip are finally ejected in the same outlet box in the experiment. For symmetry reasons, the calculation domain can be limited for the axisymmetric diffuser (grid from the axis to the wall) and for the 3D diffuser (grid on only a half domain).

The grids are generated with the CAEDS code[6] for the N3S calculation and with an orthogonal curvilinear mesh generator based on the Visbal-Knight method for the PATC[9] calculation. Table 1 gives the number of node-elements or cells for each grid.

Boundary conditions

These conditions are common to the two calculations. In the intake section, the velocity components are imposed in accordance with experimental profiles, so that the imposed values are $k=0.01U^2$ and $\varepsilon=kU$. At the walls, we use standard logarithmic laws (for U and, where applicable, T). Symmetry conditions are applied on the axis in the case of the axisymmetric diffuser and in the plane of symmetry for the 3D diffuser. In the outlet section, we use normal null stress conditions ("free outlet" conditions); this consists in considering that the pressure forces and friction forces are in equilibrium in this section.

Results: Calculations-experiments comparisons

Axisymmetric diffuser

In this configuration, PATC calculation-experiment comparisons are first made for the mean temperature profiles with strong heating ($\Delta T=380K$). Then some results obtained with the PATC and N3S codes are compared with experimental results for the velocity and the pressure in the isothermal case (the two experimental half profiles are systematically given in figures 5 to 8). In both conditions the momentum flux between the secondary and the primary flows is kept constant and corresponds to the isothermal volume flux

DIFFUSERS	GRIDS		
	PATC Point number	N3S Element number	N3S Node number (including node tops)
axisymmetric (AX)	2000	1774	3721
2D plane	1568	1721	3635
3D		4701	7437 (1110)

Table 1: Grids for the PATC and N3S codes

ratio Q_2/Q_1=0.43. In these experiments, the combination of a weak secondary flux and of the divergence of the downstream part of the diffuser (7.9°) induce a separating zone near the wall in this last part of the diffuser which particularity is the absence of a reattachment point before the diffuser outlet. Consequently, an additional air intake issuing from the outlet box comes intermittently near the diffuser wall in a reverse direction with regard to the primary flow. In order to take into account this specific feature, the boundary conditions of the PATC code have been adapted to take free outlet conditions into account. As can be seen in the results presented, this precaution greatly improved the prediction of velocity profiles, but it is still insufficient for temperature.

Figure 5 presents the axial variation of the mean temperature nondimensionalized dividing by the maximum temperature T_j at the nozzle outlet at ΔT=380K. The calculation-experiment comparison shows that the PATC code predicts more efficient mixing than in reality. However, the error is less than 5% at the diffuser outlet. Note also that the thermal core length is well described by the calculation.

Figures 6a to 6d, which show the radial profiles of mean temperature $(T-T_2)/(T_c-T_2)$ (where T_c: axis temperature, T_2: ambient temperature), confirm the calculation's prediction of more rapid spreading, particularly in the diffuser's outlet section. Nevertheless, non-negligible dissymmetries are found in the measurements. These are due to a defect in the installation's heating battery, where the flow velocity is approximately equal to the convection velocity, which induces overheating of the upper part of the flow (fig. 6a). The calculation using an intake profile based on the average experimental half-profiles is in satisfactory agreement with the experiment insofar as the numerical results are located in the middle of experimental points dispersed by dissymmetries, except at the outlet wall (fig. 6.d). This is due to under-estimation of the influence of air re-entries composed of "cold" flow that cools the diffuser walls.

The following figures, 7 and 8, correspond to results obtained in isothermal flow (ΔT=0).

Figures 7a to 7d show the radial profiles of mean longitudinal velocity non-dimensionalized by dividing by the maximal primary velocity U_j in four sections of the diffuser for experiments and the PATC and N3S codes. The N3S code is found to give better predictions of these variations, particularly for axial velocity. One also notes the slight initial dissymmetry of the experimental profiles, which is particularly accentuated in the diffuser outlet section, where the duct's divergence and the presence of recirculation flows destabilize the central flow. Figures 7c and 7d also show the conditional velocities deduced from the measurements by the hot wire/cold wire double probe that is used to evaluate the intermittence γ of the presence of reverse flow current. The technic for measurement at the pressure tube is found to be unsuitable when γ reaches 20%; beyond this value of γ, the conditional velocities are correct. In addition, very good agreement is found between these measurements at the jet edges and the numerical results.

The N3S code is shown to be more suitable for describing a flow (even 2D flow) by comparison of the calculated and experimental results given in figures 8a to 8d for radial variations of mean pressure. This is because the PATC code, which generally gives a quite good reproduction of radial variation in pressure gradient, makes a major error for its longitudinal variation when it concerns the divergent part of the diffuser (figs. 8.c and 8.d). On the other hand, the N3C code is in satisfactory agreement with experiments except for pressure variation near the axis. This is apparently due to under-estimation of the kinetic energy of turbulence, k, and poor redistribution of k among the three velocity fluctuations, particularly as the anisotropy in the initial zone of a jet is not taken into account in such models that consider the term

$p/\rho+\sqrt{(2k/3)}$ as a whole. Note that the coefficient of anisotropy v'^2/u'^2 determined here by measurements with X-crossed hot wires is 0.6 on the axis in the diffuser outlet section for turbulent intensity $u'/U_c=0.23$.

The results obtained for flow in the axisymmetric diffuser show the superiority of the N3S code in relation to the PATC code; therefore the calculation-experiment comparisons concerning velocity and pressure are only given with the N3S code hereafter.

Plane 2D diffuser

In this configuration, comparisons PATC calculation-experiment are first made for the mean temperature profiles with strong heating ($\Delta T=230K$) Then some results obtained with the N3S code are compared with experimental results for the velocity and the pressure in the isothermal case. In both conditions, the momentum flux between the secondary and the primary flows is kept constant and corresponds to the isothermal volume flux ratio $Q_2/Q_1=0.55$.

Figures 9a and 9b give the mean temperature profiles in sections 5 and 7 (cf fig. 11) of the 2D diffuser. Comparisons with N3S are obviously unfavorable since the version of the code used is not designed to describe temperature variation in cases of low heating. Comparisons with the PATC code are much more favorable. However, differences of around 15% are still found in the diffuser outlet, particularly in the zone where reverse flow occurs; this reverse flow is composed of external fresh air that is not correctly taken into account by the calculation.

Figures 10 show, for these same sections, the mean velocity measurements taken with the clinometric pressure probe and the results of the N3S code. The measurement technic employed is used to determine the mean velocity vector in terms of modulus and direction, from which we deduce the U and V components in directions X and Y (fig. 10). The experimental and numerical results both show that the flow is not equally divided on either side of the deflector in the elbow bend. In fact, the entire flow strikes against the lower wall of the diffuser and passes under the deflector, while air re-entries occur in the upper part. While the calculation slightly over-estimates the transverse velocity gradients in relation to the experiment, it complies with the distribution of flows between the upper and lower parts of the deflector. The accuracy of the N3S code in predicting flow variation in such complex conditions is confirmed by the variation of pressure on the diffuser's lower wall shown in figure 12.

3D diffuser

The results for flow in the 3D diffuser are given for a flow ratio $Q_2/Q_1=0.2$ when the "daisy section" nozzle is fitted with a central core, 30 mm in diameter, that simulates the axis of the turbine. The velocity measurements presented were taken by LDA.

Figure 13 shows the velocity component parallel to the diffuser's lower wall in section 7, in the plane of symmetry. The N3S calculation over-estimates the flow development inside the diffuser and predicts negative velocities corresponding to separation at the upper wall. This latter point is a little in disagreement with the experiment, where negative velocities can be observed using the Bragg cell. In fact, the LDA measurements indicate the presence of a "stagnant" zone near the upper wall, with minor air re-entries located around $2Y/D_2=0.3$, when the velocity becomes slightly negative. In general, therefore, the code under-estimates the extent of the recirculation zone in this section. This is not the case in section 12 at the diffuser outlet (fig. 14) where the calculation predicts exactly the start of the recirculation zone at $Z/D_2=-0.25$, even if the numerical absolute values of air re-entries are lower than the experimental values. This reflects the fact that the code predicts a more efficient mixture than in reality. Nevertheless, the flow behavior is well described, i.e. the central jet is practically not deflected by the diffuser elbow bend and strikes against its lower wall, thereby leaving room for a large recirculation zone in the upper part. The flow behavior's sensitivity to the geometrical configuration is also seen in the mean pressures at the wall, which are only determined by calculation here (fig. 15). Another noteworthy feature is that, beyond the end of the upper wall, at the horizontal abscissa 140 mm (cf fig. 17), the pressure on the diffuser wall no longer complies with that observed in a divergent duct and gradually decreases and stabilizes. This can be partly explained by the fact that the recirculation pocket limits the volume in which the jet can spread and, in a manner of speaking, it acts as a wall. According to figure 14 and the measurements in other sections (13, 14), this zone occupies practically two thirds of the diffuser outlet section (fig. 16), which is reflected by a slight convergent effect in the jet.

Figure 17 show the charts of the intensity of turbulence with a measured velocity of u'/U_j in % (the

U component is defined as the velocity component parallel to the diffuser's lower wall) in the plane of symmetry of the diffuser. The most turbulent zone is that located in the wake of the core.

Conclusion

The complexity of the flows developing in the diffuser in quasi-industrial conditions created difficulties for both the experimental and the numerical parts of this study. In the experimental work, it was necessary to employ suitable, varied and complementary measurement technics to identify the characteristics of these turbulent flows that are simultaneously subjected to pressure gradients, recirculation and strong thermal fluxes. In the numerical calculation, it was necessary to use Navier-Stokes turbulence codes while taking into account the constraints imposed by the industrial nature of the study regarding computing costs, ease of application and, of course, the reliability of the results obtained in mean fields. Comparisons of the experiments and calculations showed the superiority of the N3S three-dimensional code in relation to the PATC two-dimensional code for predicting these flows, since the PATC code was found to be deficient for the evaluation of pressure in the presence of recirculation. The N3S code was found to be a very efficient tool for predicting the behavior of such complex flows. The few deficiencies found in this code - such as its under-estimation of the extent of recirculation zones or the over-estimation of the mixture at the diffuser outlet - are normal limitations for a turbulence model using a k-ε closure. One may also consider that the prediction of the pressure on the axis is optimized in this case, since only higher order closures - particularly those using anisotropic models - could improve the results by taking into account the fact that the studied flow is in the heart of the development region. Unfortunately, to our knowledge, these types of closures are not yet available on an industrial level.

As regards temperature, the PATC code already gives satisfactory results in two-dimensional geometry. However, the introduction of the enthalpy equation in the new version (3.1) of the N3S code will make it possible to predict the behavior of strongly heated three-dimensional turbulent flows, and should produce even more conclusive results in the very near future.

Acknowledgements

The authors wish to thank the Direction des Etudes Recherches et Techniques of the French Ministry of Defense for its financial support, and Messrs. R. Dumas and M. Astier respectively for their scientific advice and technical assistance.

References

(1) AMIELH M., Thesis, Univ. Aix-Marseille II, IMST, France, (1989).

(2) CURTET R., Public. Scient. et Techn. du Ministère de l'Air, (1960).

(3) KIAN K., Doct. Thesis, Ing., INPG Grenoble, France, (1981).

(4) ZHU J., RODI W., Proc. of the Int. Symp. on Eng. Turb. Model. and Meas., Dubrovnik, Yugoslavia, (1990).

(5) AMIELH M., CHAUVE M.P., Rapport DRET/IMST 89/169, (1991).

(6) CANTILLON M., Rapport DRET/Eurocopter France 89/576, Phase II, ECF F/DF.573.34, (1993).

(7) SOLIGNAC J.L., rapport ONERA 74/1865 AN, (1984).

(8) AMIELH M., CHAUVE M.P., CORMIER F.E., 29ème Coll. d'Aérodyn. Appl., AAAF, Biscarosse, France, (1992).

(9) CANTILLON M., Thesis, Univ. Aix-Marseille I, France, (1990).

(10) CANTILLON M., Rapport DRET/Eurocopter France 89/576, Phase I, ECF n°H/DP.R.573.00, (1993).

(11) EDF, SIMULOG, Manuel théorique du code N3S, version 3.0, (1993).

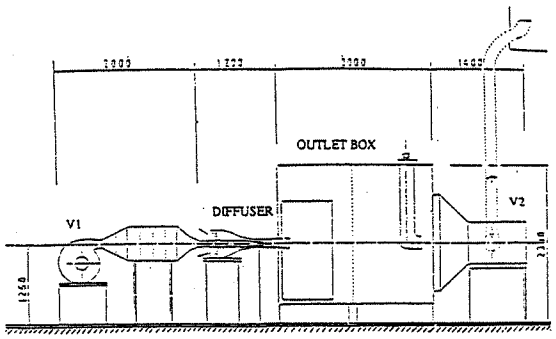

FIG.1- GENERAL VIEW OF THE EXPERIMENTAL SET-UP

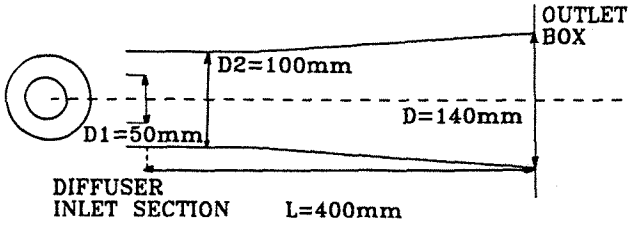

FIG.2- AXISYMMETRIC DIFFUSER (AX)

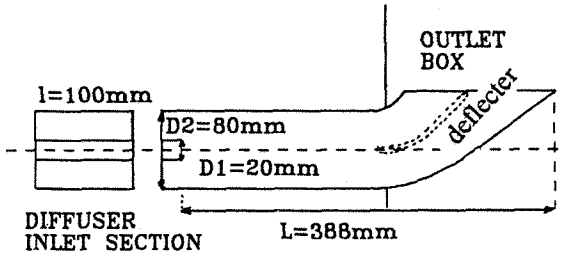

FIG.3- BIDIM. PLANE DIFFUSER (2D)

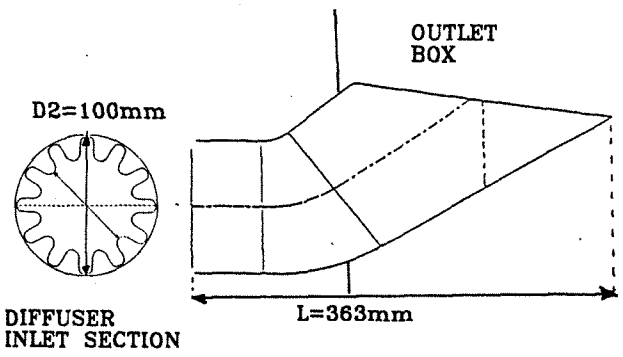

FIG.4- TRIDIMENSIONAL DIFFUSER (3D)

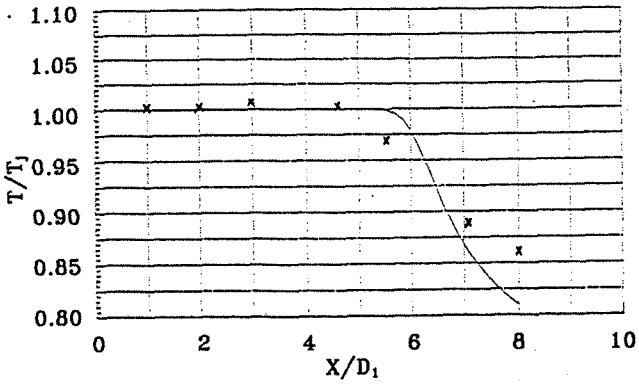

FIG.5-(AX) AXIAL DECREASE OF THE MEAN TEMPERATURE AT ΔT=380K

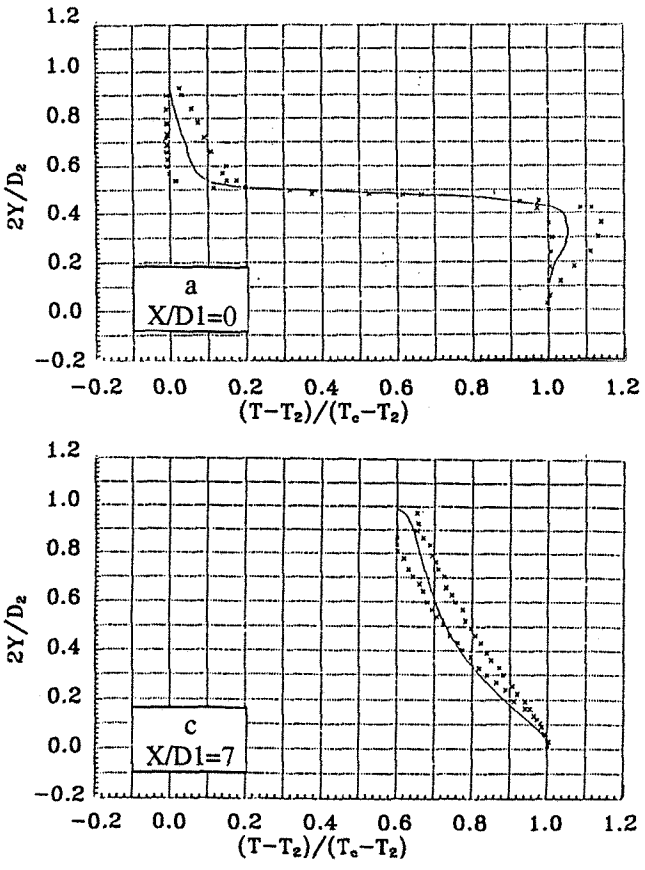

FIG.6-(AX) RADIAL PROFILES OF THE MEAN TEMPERATURE AT ΔT=380K
COMPARISONS EXPERIMENTS (EXP, x) / PATC CODE (_____)

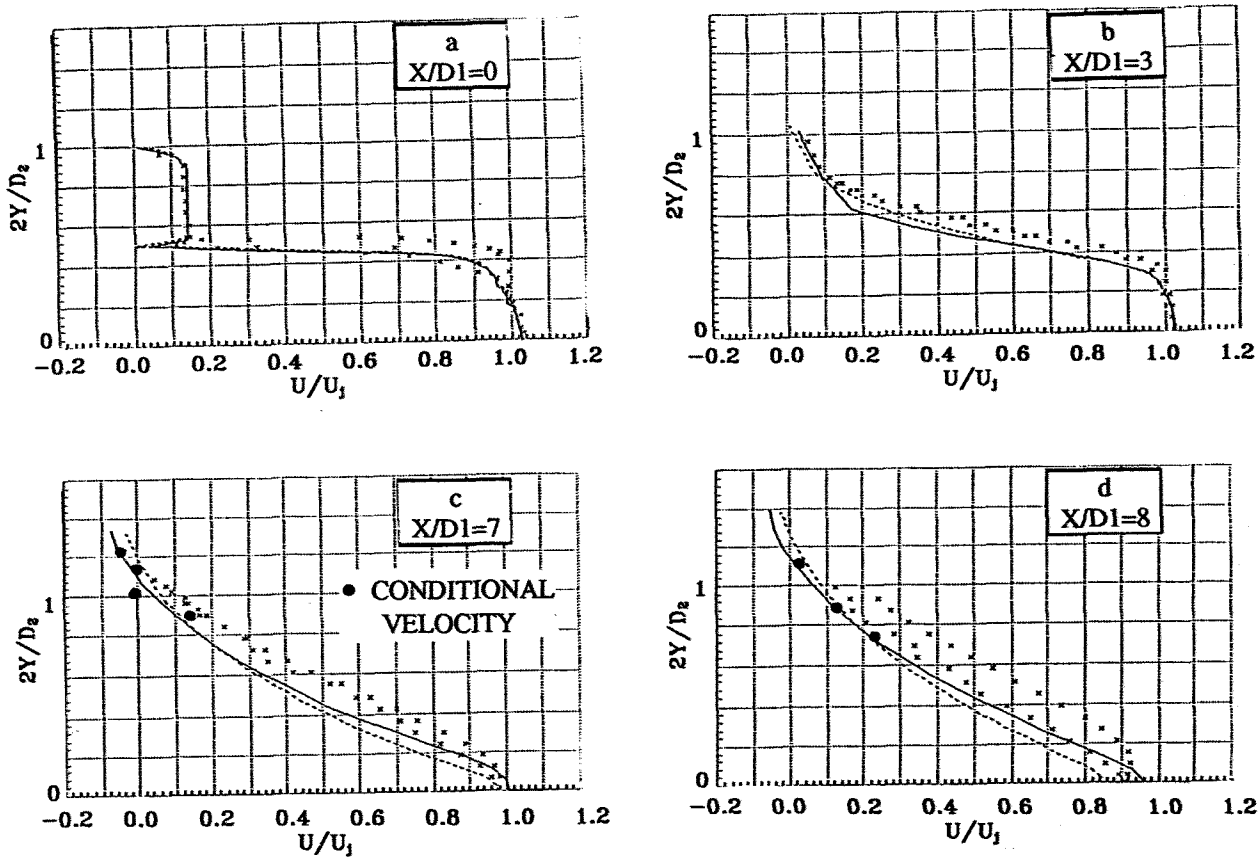

FIG.7-(AX) RADIAL PROFILES OF THE MEAN VELOCITY U AT ΔT=0
COMPARISONS EXPERIMENTS (EXP, x) / N3S CODE (____) / PATC CODE (- - - -)

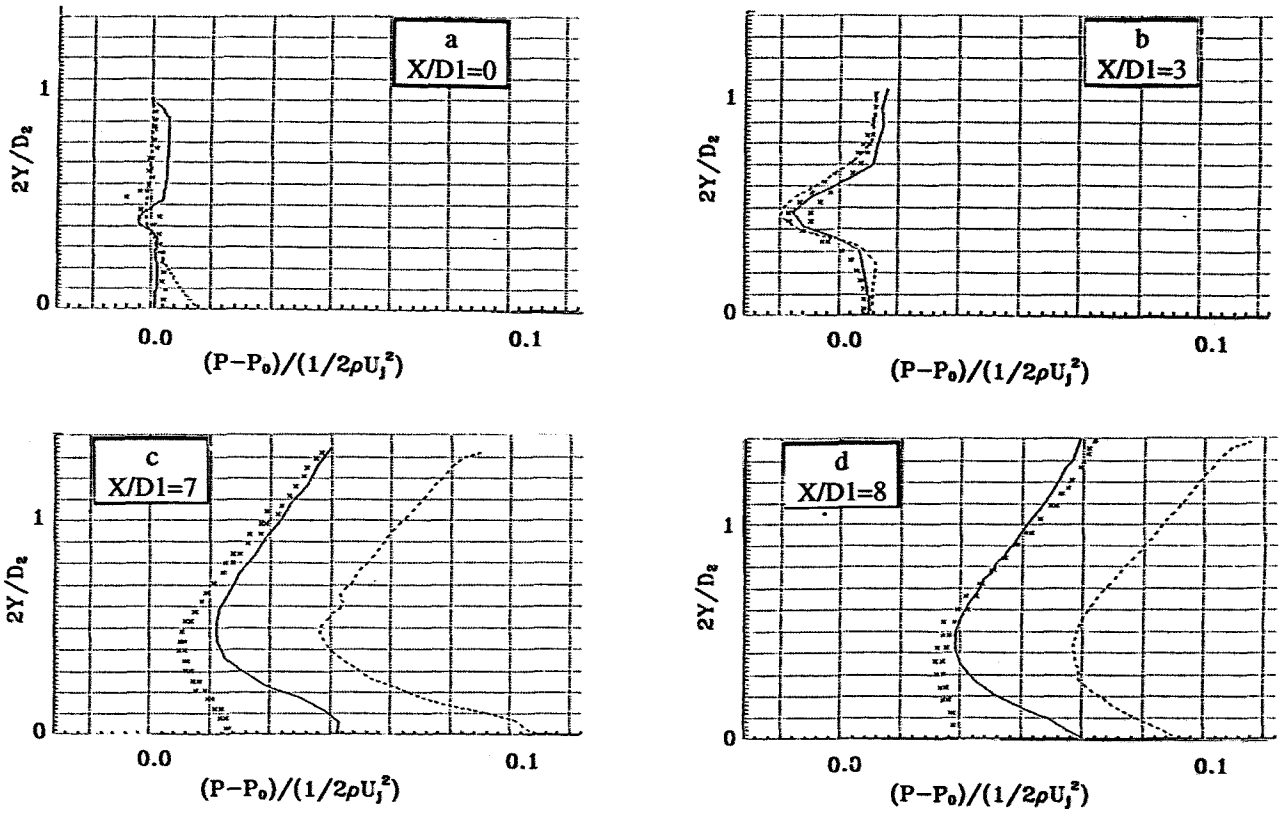

FIG.8-(AX) RADIAL PROFILES OF THE MEAN PRESSURE AT ΔT=0
SYMBOLS SEE FIG.7

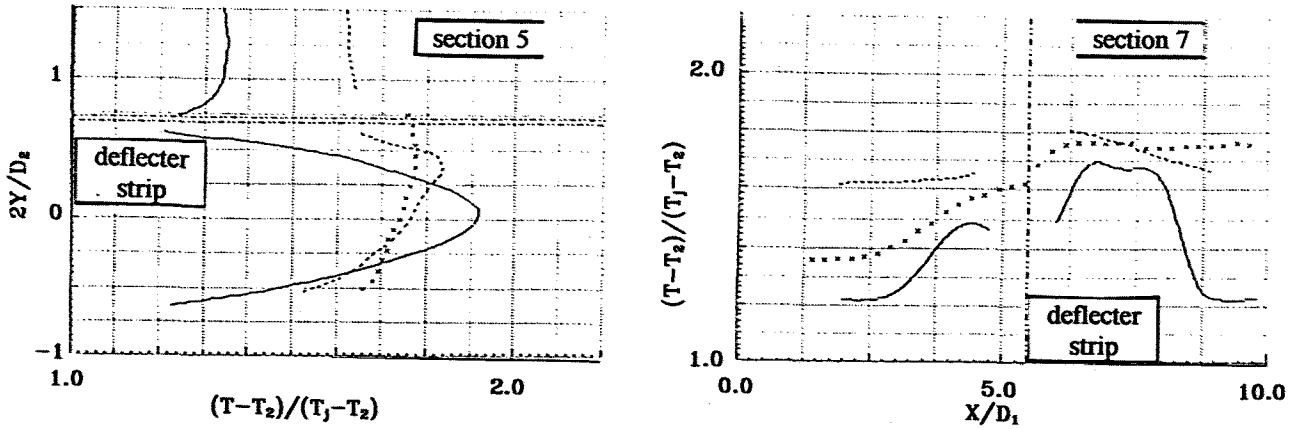

FIG.9-(2D) TRANSVERSAL PROFILES OF THE MEAN TEMPERATURE AT ΔT=230K
COMPARISONS EXP (x) / PATC CODE (----) / N3S CODE (___) IN SECTIONS 5 AND 7 (SEE FIG.11)

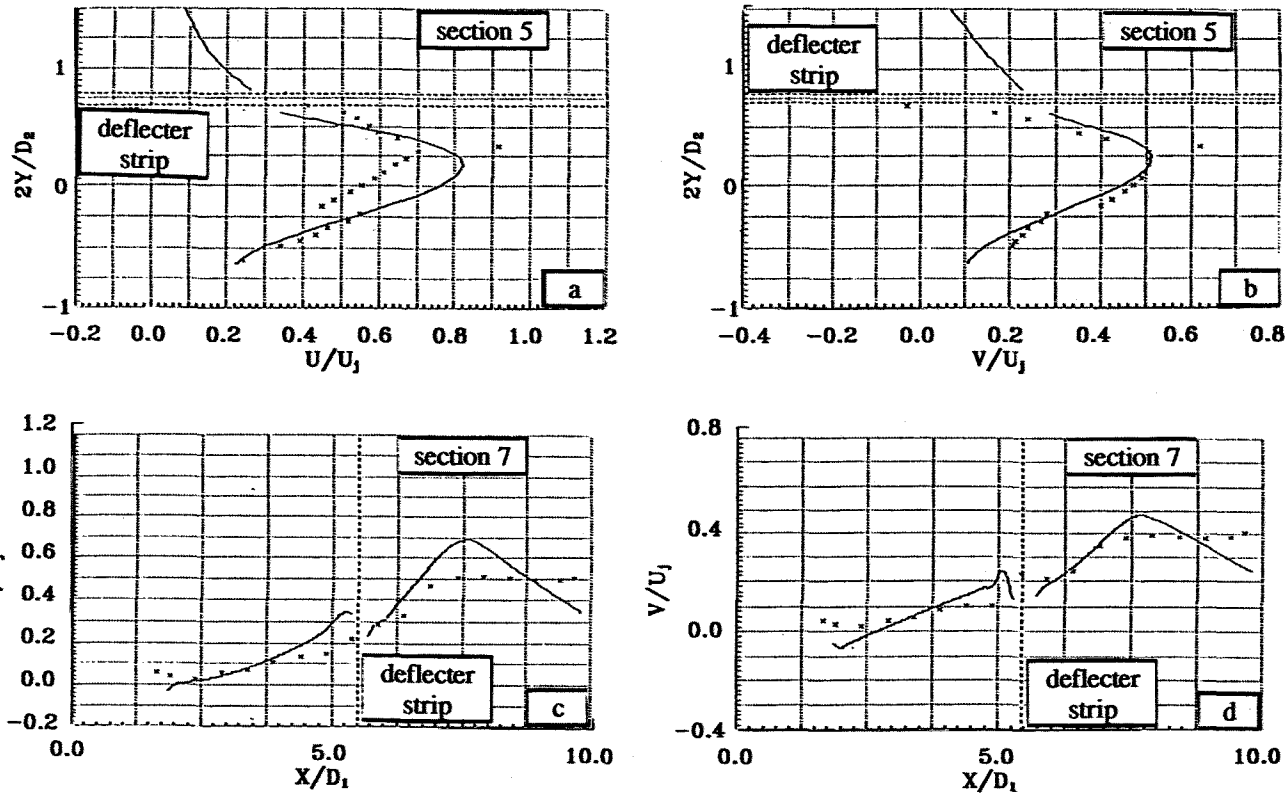

FIG.10-(2D) TRANSVERSAL PROFILES OF THE COMPONENTS U AND V OF THE MEAN VELOCITY
COMPARISONS EXP (x) / N3S CODE.(_____) IN SECTION 5 AND 7 (SEE FIG.11) AT ΔT=0

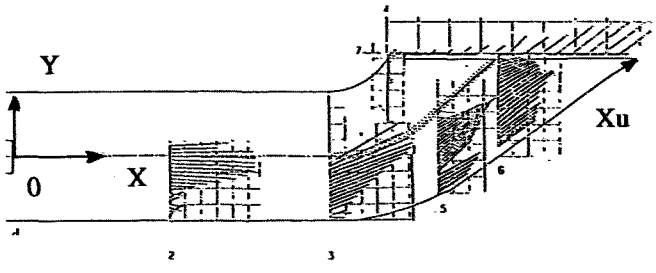

FIG.11-(2D) TRANSVERSAL PROFILES OF THE MEAN VELOCITY VECTOR AT ΔT=0 (MEASUREMENTS)

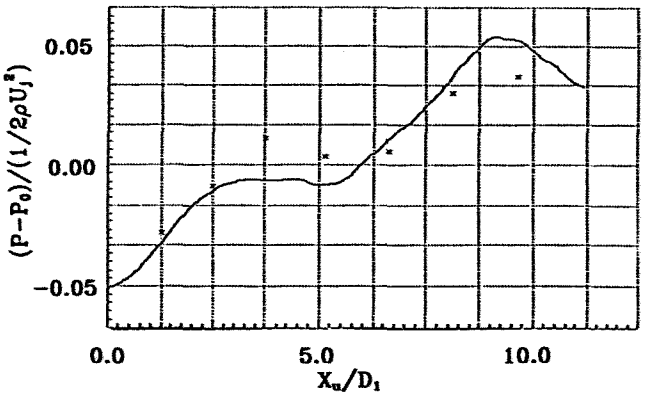

FIG.12-(2D) MEAN PRESSURE AT THE INFERIOR DIFFUSER WALL. SYMBOLS SEE FIG. 10, AT ΔT=0

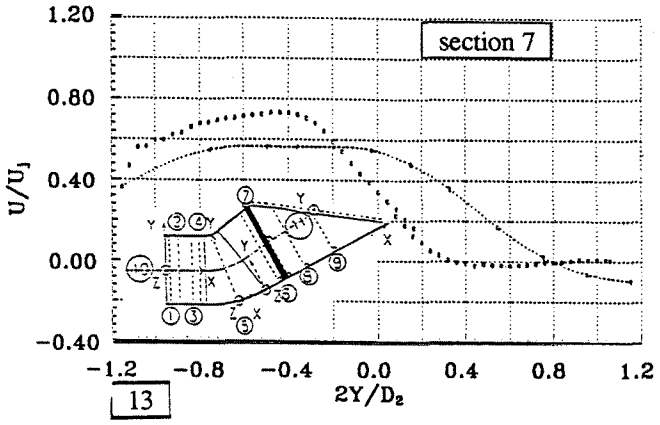

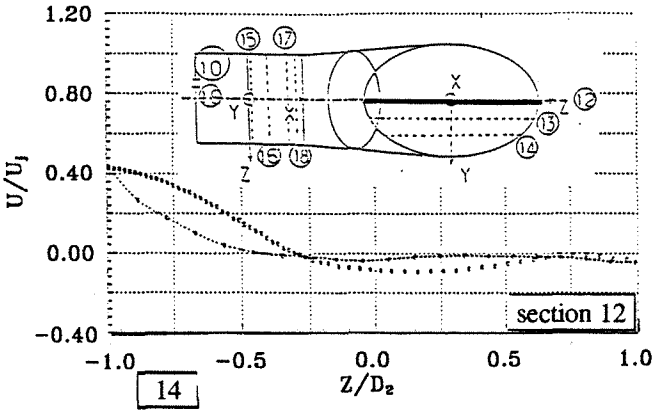

FIG.13 AND 14-(3D) TRANSVERSAL PROFILES OF THE MEAN VELOCITY COMPONENTS IN THE PLANE OF SYMMETRY. COMPARISONS LDA (o) / N3S CODE (o - o -) AT ΔT=0

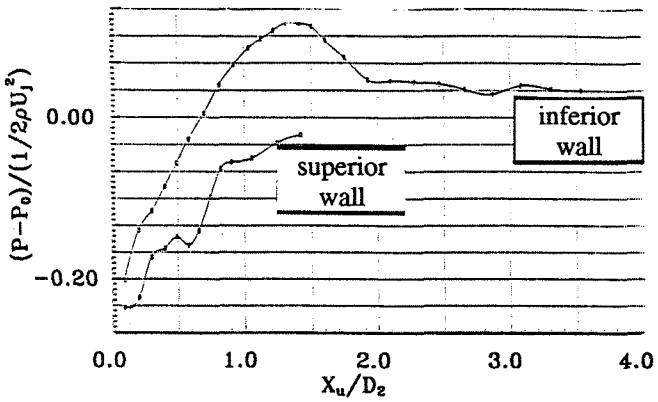

FIG.15-(3D) MEAN PRESSURE AT THE DIFFUSER WALL, AT ΔT=0, WITH N3S CODE

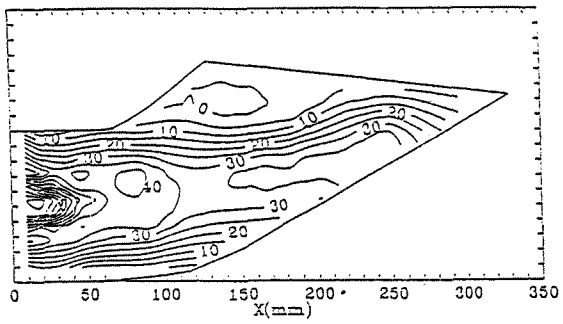

FIG.16-(3D) CARTOGRAPHY OF THE U-MEAN VELOCITY (m/s) AT ΔT=0 (LDA)

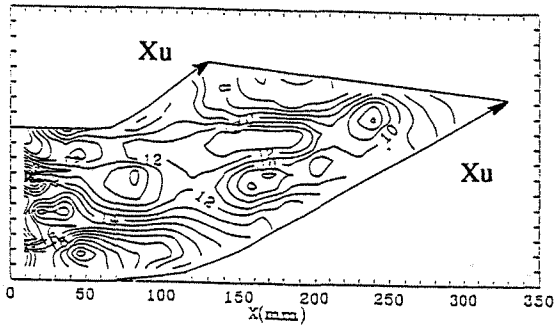

FIG.17-(3D) CARTOGRAPHY OF TURBULENT QUANTITIES EXP. (u'/Uj in %)